RAIM and Complementary Kalman Filtering for GNSS Reliability Enhancement

Helena Leppäkoski, Heidi Kuusniemi*, and Jarmo Takala
Tampere University of Technology, Finland
*Fastrax Ltd., Finland

***Abtract* - The objective of this research is to improve reliability and positioning accuracy of a mobile, standalone GNSS receiver in personal positioning. We propose a novel algorithm that fuses carrier information with code phase measurements and uses the additional security feature of receiver autonomous integrity monitoring (RAIM) and fault detection and exclusion (FDE) in order to detect and exclude erroneous measurements. The weighted least squares (WLS) method completed with RAIM/FDE is used to compute the GPS position and velocity estimates from pseudorange and delta range measurements. These estimates are combined in a complementary Kalman filter (CKF), which gives the velocity smoothed position estimate.**

The performance of the algorithm has been verified with pedestrian navigation tests; measurements for the tested algorithms were obtained using a SiRF Star II GPS receiver. Accuracy of the obtained position solutions was compared with a DGPS position solution, recorded using Thales MobileMappers. As the measure of accuracy, we used the horizontal distance of the standalone position solution from the DGPS track, i.e. the cross track error (CTE). The maximum and mean CTE values of 51.8 m and 6.3 m, respectively, were obtained with least squares (LS) position solution. With WLS and RAIM/FDE processed position, the maximum and mean errors were 25.2 m and 3.5 m. Applying CKF on WLS and RAIM/FDE processed position and velocity the values were 8.4 m and 3.1 m. Applying CKF on WLS and RAIM/FDE processed position and WLS velocity the values were 7.7 m and 2.8 m. Thus, adding the CKF to the WLS + RAIM/FDE processing reduces both the maximum and mean errors; the CKF has the largest effect on the maximum errors.

Reports of this type of CKF for fusing GPS carrier and code phase information, with the additional security feature by RAIM/FDE, do not exist in the open literature.

I. INTRODUCTION

To improve positioning accuracy in GNSS based personal positioning applications, several special characteristics need to be taken into account. The GNSS receiver needs to be inexpensive, small and light-weight; therefore only standalone GNSS positioning devices are considered in this paper. The positioning environment varies as the user moves: the amount of signal attenuation and reflections caused by constructions and vegetation varies, and signal obstructions appear and disappear frequently. The motion state of the user varies also, for instance, the user may walk, drive a car or a bicycle, or stand still. Thus the motion of the user is difficult to model using just one model.

In this paper, we propose for a mobile, standalone GPS receiver an algorithm that uses complementary Kalman filter (CKF) algorithm to fuse carrier information with code phase measurements in position domain. To solve positions and velocities, the algorithm uses weighted least squares (WLS) method with adaptively adjusted weights for measurement channels. The additional security features of receiver autonomous integrity monitoring (RAIM) and fault detection and exclusion (FDE) are used in order to detect and exclude erroneous measurements before they are fed to the filter.

This paper is organized as follows: At first, the previous work on different methods to fuse carrier and code information is discussed. Next, the design of the algorithm for position computation is described in detail. In the experimental test results, we compare the proposed algorithm with several position computation methods available for standalone GPS. The conclusions are given in the last section with remarks on future research.

The novelty in this paper is the combination of RAIM/FDE processing to a complementary Kalman filter and application of this combination to process data of a standalone, single-frequency GPS receiver.

II. PREVIOUS WORK

The synergism of code and carrier measurements offers possibilities to improve the positioning accuracy of a standalone receiver. When compared to a code phase measurement, the carrier phase measurement is less noisy, but gives only relative information; initial range or phase ambiguities need to be solved using code phase measurements. Several methods for combining carrier and code information have been described in the literature. One category of known methods consists of different forms of carrier smoothing [1-3]. Another main category of methods utilizes centralized Kalman filter with motion models [4, 5]. For personal positioning applications, both the carrier smoothing and centralized filter with motion model have their shortcomings.

Typically in the carrier smoothing schemes, there is an independent filter for each receiver channel. The filter performs the smoothing of the pseudorange measurements using delta pseudorange or phase range information and outputs smoothed pseudorange estimates, from which the position estimate is computed. In channel-wise carrier smoothing, a loss of phase lock during signal tracking causes

H. Leppakoski, H. Kuusniemi and J. Takala, "RAIM and Complementary Kalman Filtering for GNSS Reliability Enhancement," 2006 IEEE/ION Position, Location, And Navigation Symposium, 2006, pp. 948-956.
doi: 10.1109/PLANS.2006.1650695

re-initialization of the filter: the estimate restarts from the accuracy of the code phase measurement and then gradually improves if the phase lock is maintained. In urban and suburban environments, signal obstructions appear and disappear frequently as the user moves. In carrier smoothing, these visibility discontinuities cause frequent losses of phase lock and thus frequent resets of the filters that are used to compute the carrier smoothed pseudorange estimates.

When centralized Kalman filter in non-complementary form is used to combine the information of carrier and code measurements, both measurements are fed to the filter as measurement updates. The time projection of the state is done using motion models, which describe the motion of the user as random process. In personal positioning applications, motion characteristics of the user may vary a lot. A proper model suitable for all possible motion states of the user is not easy to find. An attempt to use one motion model to cover all the possible motion states may easily lead to a solution that does not describe well any of the motion states. Some multiple model approach may work properly, as stated e.g. in [6], but such approaches would lead to more complex algorithm and laborious tuning process of different models and model change probabilities.

To mitigate the problem of frequent filter resets, a fusion filter was proposed in [7]. Instead of smoothing pseudoranges with carrier measurements, the filter uses carrier based GPS velocity estimates to smooth the pseudorange based GPS position. With over-determined Weighted Least Squares (WLS) solutions of position and velocity, effect of the independent channel noises is suppressed. Weights for each satellite channel are adjusted adaptively as functions of carrier-to-noise ratios (C/N_0). The WLS solutions of position and velocity are processed with a fusion filter that further attenuates the effect of the remaining noises. The filter structure is a complementary Kalman filter (CKF): the velocity estimate is used to propagate the state. Thus, no motion model is required in the filter implementation, i.e. the filter design is independent of the motion state of the user. The GPS position estimate is fed to the filter as a measurement and the output of the filter is the smoothed position. With this procedure, the total filter reset occurs only when the number of visible satellites drops below four. The complementary filter configuration applied to a linear problem in [7] is similar to a configuration that was proposed for nonlinear problems in [8]. A similar configuration has been used also for differential GPS (DGPS) in [9], where the filter was used to process information of code and carrier double differences. In [10], the configuration was applied to GPS/INS integration.

In the filtering approach, e.g., in [7], the measurement weighting and complementary filtering are the only means to attenuate measurement noises. This introduces drawbacks in urban and suburban environments where both the code and carrier measurement may occasionally be deteriorated by large errors due to unexpected effects of multipath attenuation. Such large errors do not fit to the noise models used by the filter, i.e., they are measurement outliers that may result into large errors in the filter state if they are allowed to affect the filter.

In this paper, we enhance the algorithm from [7] to include also RAIM/FDE for detection and exclusion of the measurement outliers before they enter the filtering process. If there are redundant pseudorange and delta pseudorange measurements available for position and velocity computations, the consistency of the measurements is examined using the RAIM/FDE procedure. The aim is to detect and exclude outliers from the measurement set that is used in the computation of position and velocity. The filtering part does not require stochastic modeling of the user motion. Unlike the previously reported complementary filter approaches to GPS positioning, this filter is independent of other sources, i.e., it does not require external sensor information or information from reference receivers. This filter differs from various carrier-smoothing approaches as it combines the information of carrier and code phase information in position domain instead of channel wise processing in line of sight coordinates.

III. OVERWIEV OF THE SYSTEM

The overview of the proposed signal processing system is shown in Fig. 1. C/N_0 values of the satellite channels are used to estimate noise variances of the measurements. The WLS method completed with RAIM/FDE is used to compute the GPS position and velocity estimates from pseudorange and delta pseudorange measurements. The RAIM/FDE processed WLS estimate of the position is fed to the complementary Kalman filter (CKF) as a measurement signal; the RAIM/FDE processed WLS estimate of the velocity is used to propagate the state. The states and the output of the fusion filter are the smoothed position coordinates of the user.

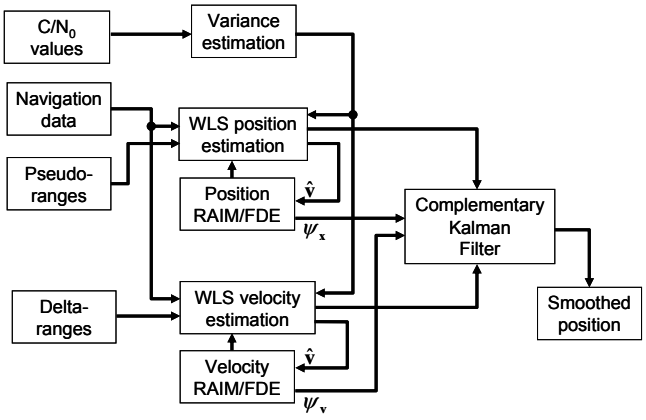

Fig. 1. An overview of the proposed signal processing system.
ψ_x : Binary position RAIM/FDE output (1=successful, 0=unsuccessful)
ψ_v : Binary velocity RAIM/FDE output (1=successful, 0=unsuccessful)

IV. ESTIMATION OF MEASUREMENT NOISE VARIANCES

To estimate the uncertainty of the pseudorange observations, we used the following equation:

$$\sigma_\rho^2 = \sigma_{tDLL}^2 + \sigma_{atm}^2 \quad (1)$$

where σ_{tDLL} is the 1-sigma thermal noise in delay lock loop (DLL) of the receiver and σ_{atm} is 1-sigma value of the uncertainties due to the atmosphere. The thermal noise component can be written as a function of carrier to noise ratio c/n_0 [9]:

$$\sigma_{tDLL} = \lambda_c \sqrt{\frac{4F_1 d^2 B_n}{c/n_0}\left[2(1-d) + \frac{4F_2 d}{T\, c/n_0}\right]} \quad (2)$$

where we used the following parameters: discriminator correlator factor $F_1 = 1$, discriminator type factor $F_2 = 1$, correlator spacing $d = ½$ [chips], code loop noise bandwidth $B_n = 2$ [Hz], predetection integration time $T = 2$ [ms] and GPS propagation constant / code chipping rate $\lambda_c = 293.05$. In [9], the error budget of the SPS C/A-code pseudorange gives the values 5.0 m and 1.5 m for 1-sigma values of ionospheric and tropospheric delays, respectively. Their summed effect is 5.22 m, which was used as the σ_{atm} value in (1).

The 1-sigma value of phase lock loop (PLL) measurement error is a sum of several noise contributions, which depend much on the receiver implementation. The 1-sigma values for PLL thermal noise can be estimated using the following equation [9]:

$$\sigma_{tPLL} = \lambda_{L1} \sqrt{\frac{B_n}{c/n_0}\left[1 + \frac{1}{2T\, c/n_0}\right]} \quad (3)$$

where we used the following parameters: code loop noise bandwidth $B_n = 18$ [Hz], predetection integration time $T = 2$ [ms], GPS propagation constant / L-band carrier frequency $\lambda_{L1} = 0.1903$ [cycles/s]. The delta pseudorange observation often includes some low frequency components due to the drifts in the measurement process of the receiver and slowly changing atmospheric effects. For this reason we overestimated the covariance of the errors as

$$\sigma_\delta^2 = 0.03^2 + \left(10\sigma_{tDLL}\right)^2 \quad (4)$$

The variance estimates σ_ρ^2 and σ_δ^2 are computed for each receiver channel with measurements and these values are used as adaptive weights in WLS computation of position and velocity.

V. POSITION AND VELOCITY COMPUTATION

A detailed description of position and velocity computation using the WLS method is given in [7]. The WLS method to solve linear systems with noisy measurements is described e.g. in [11], the equations for LS solution of position and velocity are given in e.g. [9] and the relation between range rate and Doppler frequency can be found in [12].

In position equation, the four unknown variables, i.e., three position coordinates and clock bias of the receiver are arranged to vector $\mathbf{x} = [x_u, y_u, z_u, -ct_u]^T$. The relation between the unknowns and the pseudorange measurements is defined by the following:

$$\rho_j(\mathbf{x}) = \sqrt{(x_j - x_u)^2 + (y_j - y_u)^2 + (z_j - z_u)^2} + ct_u \quad (5)$$

where j is the index of measurement channel, (x_j, y_j, z_j) is the position of the jth satellite tracked by the receiver and c is the speed of light. If pseudorange measurements of at least four satellites are available, the unknown variables can be computed using

$$\hat{\mathbf{x}} = \mathbf{x}^* + \Delta\mathbf{x} \quad (6)$$

where $\mathbf{x}^*$ is the linearization point of the pseudorange equations and $\Delta\mathbf{x}$ is the WLS solution of the linearized pseudorange equations, computed using

$$\Delta\mathbf{x} = \left(\mathbf{H}^T \boldsymbol{\Sigma}_\rho^{-1} \mathbf{H}\right)^{-1} \mathbf{H}^T \boldsymbol{\Sigma}_\rho^{-1} \Delta\boldsymbol{\rho} \quad (7)$$

where $\mathbf{H}$ is the measurement matrix, also known as design matrix, which is a result of the linearization of the pseudorange equations (5). The weight matrix is the inverse of the diagonal matrix $\boldsymbol{\Sigma}_\rho$. The diagonal elements of $\boldsymbol{\Sigma}_\rho$ are the variances of pseudorange measurements, estimated using (1). The column vector $\Delta\boldsymbol{\rho}$ is the difference between measured pseudoranges and estimated pseudoranges, i.e., $\Delta\boldsymbol{\rho} = \boldsymbol{\rho}(\mathbf{x}) - \boldsymbol{\rho}(\mathbf{x}^*)$.

In velocity equation, the four unknown variables, i.e., three components of the user velocity and clock drift of the receiver are arranged to vector $\dot{\mathbf{x}} = \left[\dot{x}, \dot{y}, \dot{z}, -c\dot{t}_u\right]^T$. The velocity components of the jth satellite are arranged to vector $\dot{\mathbf{x}}_j = \left[\dot{x}_j, \dot{y}_j, \dot{z}_j, 0\right]^T$. The WLS solution of velocity is computed using

$$\hat{\dot{\mathbf{x}}} = \left(\mathbf{H}^T \Sigma_{\dot{\rho}}^{-1} \mathbf{H}\right)^{-1} \mathbf{H}^T \Sigma_{\dot{\rho}}^{-1} \mathbf{d} \quad (8)$$

where $\mathbf{H}$ is the same matrix as in (7) and $\Sigma_{\dot{\rho}}^{-1}$ is the weight matrix based on the error variances of range rate measurements, estimated using (4). The elements of the column vector $\mathbf{d}$ are computed using

$$d_j = -\dot{\rho}_j + \mathbf{h}_j \dot{\mathbf{x}}_j \quad (9)$$

where $\dot{\rho}_j$ is the range rate measurement of the jth satellite. It is a function of the Doppler frequency, i.e., the difference between the received frequency f_j and transmitted frequency f_{Tj}: $-\dot{\rho}_j = c\left(f_j - f_{Tj}\right) / f_{Tj}$. The row vector $\mathbf{h}_j$ is the jth row of the matrix $\mathbf{H}$.

If the observable is the delta pseudorange measurement $\delta\rho_j$ instead of the rate range, the WLS method can be used to solve the delta position, i.e., the position change within a sampling interval:

$$\boldsymbol{\delta}\hat{\mathbf{x}} = \left(\mathbf{H}^T \boldsymbol{\Sigma}_{\delta\rho}^{-1} \mathbf{H}\right)^{-1} \mathbf{H}^T \boldsymbol{\Sigma}_{\delta\rho}^{-1} \mathbf{g} \quad (10)$$

where $\boldsymbol{\Sigma}_{\delta\rho}^{-1}$ is the weight matrix based on the error variances of delta pseudorange measurements, estimated using (4). The elements of the column vector $\mathbf{g}$ are computed using

$$g_j = -\delta\rho_j(t_k) + \int_{t_{k-1}}^{t_k} \mathbf{h}_j \mathbf{v}_j \, dt \,. \tag{11}$$

The delta pseudorange is defined as

$$\delta\rho_j(t_k) = \int_{t_{k-1}}^{t_k} \dot{\rho}_j \, dt \tag{12}$$

where $t_{k\text{-}1}$ and t_k are the start and end times of the kth sampling interval. The integral term in (11) can be approximated using the average of the satellite velocities at sampling instances:

$$\int_{t_{k-1}}^{t_k} \mathbf{h}_j \mathbf{v}_j \, dt \approx \mathbf{h}_j(t_k) \frac{\mathbf{v}_j(t_{k-1}) + \mathbf{v}_j(t_k)}{2} \left[t_k - t_{k-1}\right] \tag{13}$$

The solution of (10) is readily in the form required by the complementary filter for smoothing the position estimate. If solution of (8) is used, the delta position must be approximated using numerical integration – the simplest approximation is obtained by multiplying the velocity estimate by Δt, the length of the sampling instance. In the following, we use the word 'velocity' to refer to the solutions of both (8) and (10), as they both are related to the velocity; the first one is approaching instantaneous velocity as it is measured over a short time interval, the latter can be scaled to represent the average velocity between the sampling instances.

The variances of position, velocity and delta position estimates are computed using the following:

$$\mathbf{P} = \left(\mathbf{H}^T \mathbf{\Sigma}^{-1} \mathbf{H}\right)^{-1} \tag{14}$$

where $\mathbf{\Sigma}$ is the corresponding weight matrix $\mathbf{\Sigma}_\rho, \mathbf{\Sigma}_{\dot{\rho}}$ or $\mathbf{\Sigma}_{\delta\rho}$.

VI. Reliability Monitoring – RAIM/FDE

Reliability refers to the controllability of observations – the ability to detect blunders and to estimate the effects that undetected blunders may have on a solution [13]. In this paper, reliability monitoring consists of reliability testing, i.e., detecting and identifying a measurement error, as in Receiver Autonomous Integrity Monitoring (RAIM), e.g., in [14].

The advantage in using parameter estimation and actually treating the observations as random values rather than computing a unique solution from just as many observations as necessary is to have access to the redundancy which is the basis of both improved precision and quality control. Assuming a correct measurement model, observational residuals defined as the difference between the estimated values of the observations and their corresponding measured values indicate the extent to which the measurements agree with each other. Residuals are, therefore, useful for monitoring the quality of the estimated parameters. When redundant observations have been made, least squares residuals of the pseudoranges or alternatively pseudorange rates can be obtained as

$$\hat{\mathbf{v}} = \mathbf{H}\hat{\mathbf{x}} - \mathbf{y} = -\mathbf{R}\mathbf{y} \tag{15}$$

where $\mathbf{H}$ is the design matrix, $\hat{\mathbf{x}}$ is the estimate of the unknown user parameters (offset from the linearization point or user velocity), $\mathbf{R}$ is a projector from the reduced observations $\mathbf{y}$ to the least squares (LS) residuals. The resulting residual vector, $\hat{\mathbf{v}}$, is thus the difference between the predicted measurements based on the least squares estimate and the empirical measurements, and it can be used to test the internal consistency among the observations. The vector can also be used to check the validity of the assumptions underlying the used functional and stochastic models and further to detect and identify a potential model error. An a posteriori variance factor can be composed based on the residuals as

$$\hat{\sigma}_0^2 = \frac{\hat{\mathbf{v}}^T \mathbf{\Sigma}^{-1} \hat{\mathbf{v}}}{n - p} \tag{16}$$

where the matrix $\mathbf{\Sigma}$ represents the covariance matrix of the observations, n represents the number of available observations, and p denotes the number of unknowns to be estimated. The a posteriori variance describes the consistency between the estimate and the measurements. The residuals, the vector $\hat{\mathbf{v}}$, can also be standardized as

$$w_i = \left| \frac{\hat{\mathrm{v}}_i}{\sqrt{\left(\mathrm{C}_{\hat{\mathrm{v}}}\right)_{ii}}} \right| \quad , i = 1:n \tag{17}$$

where $\hat{\mathrm{v}}_i$ denotes the ith element of the residual vector, and $\left(\mathrm{C}_{\hat{\mathrm{v}}}\right)_{ii}$ denotes the ith diagonal element of the covariance matrix of the residuals, $\mathbf{C}_{\hat{\mathbf{v}}}$. The standardized residuals can be used for outlier detection with uncorrelated, normally distributed observations in a sense that if the ith observation is not an outlier, w_i is normally distributed as $w_i \sim \mathrm{N}(0,1)$ [13, 15]. The covariance matrix of the residuals is computed as follows

$$\mathbf{C}_{\hat{\mathbf{v}}} = \mathbf{\Sigma} - \mathbf{H}\left(\mathbf{H}^{\mathrm{T}} \mathbf{\Sigma}^{-1} \mathbf{H}\right)^{-1} \mathbf{H}^{\mathrm{T}} \tag{18}$$

Moreover, for the projector matrix, the following equation can be derived

$$\mathbf{R} = \mathbf{C}_{\hat{\mathbf{v}}} \mathbf{\Sigma}^{-1} \tag{19}$$

The trace of this matrix $\mathbf{R}$ is the overall redundancy (degree of freedom), and, therefore, $\mathbf{R}$ is referred to as 'redundancy matrix', e.g., [16]. With uncorrelated observations, this matrix plays a key role in quality control. The ith diagonal element of matrix $\mathbf{R}$, r_i, corresponds to the contribution of the ith observation to the overall redundancy, but it is also the scale factor with which a bias of an observation will be reflected by its residual [17]. A balanced adjustment problem would have all the diagonal elements of the redundancy matrix approximately equal. When r_i is close to zero, the ith observation contributes very little to the redundancy, which also implies that it is hardly controlled by the other observations. Thus, very small redundancy numbers are not desirable. A zero redundancy number implies an uncontrolled observation.

The effect, $\nabla_i \hat{\mathbf{v}}_i$, of an error $\nabla \mathbf{y}_i$ in observation $\mathbf{y}_i$ onto its corresponding residual is determined by the *i*th diagonal element of **R** [17], i.e.,

$$\nabla_i \hat{\mathbf{v}}_i = -r_i \nabla \mathbf{y}_i \tag{20}$$

Since r_i is always between 0 and 1 [17, 13], possibly only a small part of an error shows up in the residuals, while the rest of it will be absorbed in the determination of the unknown parameters. An error in an observation that has a large redundancy number will affect the corresponding residual more directly and is easier to detect. The effect of a gross error $\nabla \mathbf{y}_i$ in observation $\mathbf{y}_i$ onto the other residuals $\hat{\mathbf{v}}_j (j \neq i, j = 1:n)$, $\nabla_i \hat{\mathbf{v}}_j$, is determined by the off-diagonal elements (r_{ji}) of the redundancy matrix **R** as

$$\nabla_i \hat{\mathbf{v}}_j = -r_{ji} \nabla \mathbf{y}_i, \quad j \neq i, j = 1:n \tag{21}$$

Thus, due to the correlation of the residuals, a gross error in an observation might have spread over all of the residuals. If a blunder is large enough to cause many reliability test failures, resulting in many alternatives, it is essential to ensure that any two alternatives are separable [18]. Therefore, in order to pinpoint the erroneous observation $\mathbf{y}_i$ through examination of its corresponding residual $\hat{\mathbf{v}}_i$, the following equation must be assessed [17]:

$$r_i > \left| r_{ji} \right| \quad (j \neq i, j = 1:n) \tag{22}$$

If the above equation does not hold, localization of the gross error is difficult.

VII. Failure Detection and Isolation

To detect a measurement error, the least squares residuals can be statistically tested. In a 'global test', the null-hypothesis H_0 states that the adjustment model is correct and the distributional assumptions meet the reality, as opposed to the alternative H_a which states that the adjustment model is not correct. If the global test fails, a 'local test' with more specific alternative hypotheses needs to be performed for failure isolation.

A. Global Test

The global test for detecting an inconsistent adjustment model is based on the quadratic form $\hat{\mathbf{v}}^{\mathrm{T}} \boldsymbol{\Sigma}^{-1} \hat{\mathbf{v}}$ which follows a central chi-square distribution with (*n*-*p*) degrees of freedom, if the observation errors are normally distributed as $\mathrm{N}(\mathbf{0}, \boldsymbol{\Sigma})$. The parameter *p* denotes the number of parameters to be estimated. If the test statistic exceeds the threshold $\chi^2_{1-\alpha, n-p}$, where α represents the false alarm rate, H_0 is rejected in favor of H_a. In this case, an inconsistency in the assessed observations is assumed, and the error should be identified and mitigated.

B. Local Test

The most likely reason for the rejection of H_0 is the presence of outlying observations. Strict testing is easy under the assumption that there is only one outlier in the current epoch. The attempt to identify such an individual measurement error may be performed if the redundancy is at least two. Each standardized residual w_i is compared to the α_0-quantile of the standard normal distribution, $\mathrm{n}_{1-\frac{\alpha_0}{2}}$, with the predetermined false alarm rate α_0. The null-hypothesis $H_{0,i}$, which denotes that the *i*th observation is not an outlier, is rejected if w_i exceeds the threshold. The underlying assumptions of the local test include that the model and the assumption of a normally distributed error vector, i.e., $\boldsymbol{\varepsilon} \sim \mathbf{N}(\mathbf{0}, \boldsymbol{\Sigma})$, are correct except for the single constant bias of the *i*th observation. The standardized residuals are then normally distributed with zero expectation when $H_{0,i}$ is correct, and with a non-zero expectation otherwise. Thus, the local testing is based on the comparison

$$w_i \leq \mathrm{n}_{1-\frac{\alpha_0}{2}} \tag{23}$$

with rejection of $H_{0,i}$ (i.e. recognition of $H_{a,i}$) if the critical value is surpassed.

Only if H_0 of the global test is rejected, the local test is carried out for fault identification, and only the observation with the largest value of w_i is tested and possibly rejected. This is a reliability testing or outlier detection procedure introduced originally by Baarda in 1968 [19]. It is known as data snooping.

The risk level α of the global test must relate to that of the local test, α_0, together with the probability β of missed detection, which is the same for both the global and the local tests. An erroneous measurement that causes the global test to fail should be indicated by the corresponding local test with the same probability. So, only two of the values α, α_0, and β can be chosen arbitrarily. They are linked by the following equations:

$$\lambda = \delta_0^{\,2} = \left(\mathrm{n}_{1-\frac{\alpha_0}{2}} + \mathrm{n}_{1-\beta} \right)^2 \tag{24}$$

$$\chi^2_{(\beta,\, n-p,\, \lambda)} = \chi^2_{(1-\alpha,\, n-p)} \tag{25}$$

where λ is the non-centrality parameter of a non-central chi-square distribution related to the global hypothesis testing and δ_0 is the expected value of the normal distribution related to the local test.

The assumption of a single outlier seems to be a severe restriction. However, it was found that data snooping can also cope with multiple blunders if it is performed iteratively. After exclusion of an observation, the parameter estimation, global and local statistical tests, and possibly the rejection of an observation can be repeated for that epoch until no more outliers can be identified.

C. Fault Detection and Exclusion

If m outliers are suspected, generally, a redundancy of at least $m+1$ is needed in order to possibly identify them. However, due to the mutual influence of observations, i.e., an error of one observation is absorbed by the residuals of all observations, erroneous rejection of a good observation is possible, especially with large or multiple biases [20]. In degraded signal environments, the redundancy is generally poor and, thus, it is desired to retain as many observations as possible to obtain an efficient estimate [21-23]. Therefore, if more than one observation is being excluded, the iterated reliability checking process should include a reconsideration of an earlier rejected observation [24].

The flowchart in Fig. 2 expresses the fault detection and exclusion procedure chosen based on the global and local statistical testing for the application of this paper, and it is called the Forward-Backward FDE. The Forward-Backward FDE method involves use of the global test to identify an inconsistent solution, and performing the local test to identify and exclude the erroneous measurement. The exclusion is, however, not performed if there is another observation that is more influential than the one subject to assessment. Thus, in FDE execution, no other more influential observation may be tolerated: when pinpointing the observation i to be excluded, it should be excluded from the solution only if the ith redundancy number r_i follows the equation $r_i > |r_{ji}| \quad (j \neq i, j = 1:n)$. The global test and the local test with the additional influentiality check are performed recursively until no more erroneous measurements are found and the solution is declared as either reliable or unreliable. In addition, the reconsideration of an earlier rejected observation is included in the Forward-Backward FDE scheme, as presented in **Fig. 2** [25]. This is performed by reconsidering all of the excluded measurements and performing global tests to find the measurements that can be implemented back into the solution computation. Thus, a measurement that has been excluded earlier is used again for the solution computation if the global test passes upon its tentative inclusion into the solution estimation. This is done to ensure that the order of the excluded measurements does not cause an unnecessary exclusion. Due to the importance of the measurements to the geometry of the solution, it is desirable to minimize the number of unnecessary exclusions.

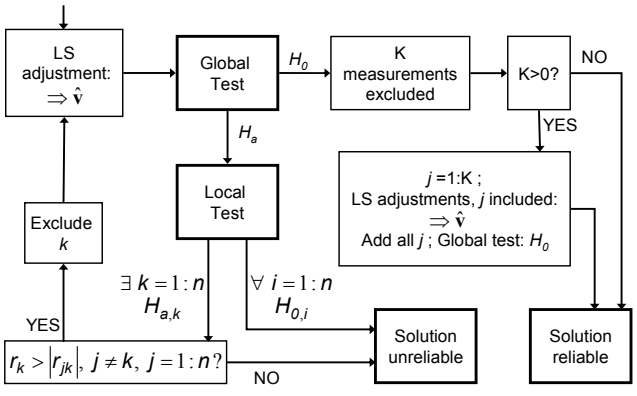

Fig. 2. Forward-Backward FDE

VIII. Complementary Kalman Filter

There are two different types of measurement sets available for computing the smoothed position estimate. The first measurement is the RAIM/FDE processed delta position, corrupted by white noise:

$$\begin{aligned}\mathbf{z}_1(t_k) &= \int_{t_k}^{t_{k+1}} \dot{\mathbf{x}}(t)\,dt + \boldsymbol{\varepsilon}_{\delta x}(t_k) \\ &= \mathbf{x}(t_{k+1}) - \mathbf{x}(t_k) + \boldsymbol{\varepsilon}_{\delta x}(t_k) \\ &= \delta\mathbf{x}(t_k) + \boldsymbol{\varepsilon}_{\delta x}(t_k)\end{aligned} \tag{26}$$

where $\mathbf{x}$ is position, t_{k+1} is the time of the last measurement sample, t_k is the time of the previous measurement sample and $\boldsymbol{\varepsilon}_{\delta x}$ is the measurement noise. The second measurement is the RAIM/FDE processed position, corrupted by white noise $\boldsymbol{\varepsilon}_x$:

$$\mathbf{z}_2(t_k) = \mathbf{x}(t_k) + \boldsymbol{\varepsilon}_x(t_k) \tag{27}$$

The goal of the fusion filter is to blend optimally together the information of the two measurements. One obvious solution would be a Kalman filter (KF) with position $\mathbf{x}$(t) as the state variable and $\mathbf{z_1}$ and $\mathbf{z_2}$ as the measurement signals. In this alternative, the velocity $\dot{\mathbf{x}}(t)$ need to be modeled as a random process. The problems of this design were discussed in section II. To avoid modeling the velocity, we use complementary filter configuration proposed in [7], where one measurement is used to propagate the state and the other provides the measurement update. The filter equations are the following:

Time projection:

$$\hat{\mathbf{x}}^-(t_k) = \hat{\mathbf{x}}(t_{k-1}) + \mathbf{z}_1(t_k) \tag{28}$$

$$\mathbf{P}^-(t_k) = \mathbf{P}(t_{k-1}) + \mathbf{Q}(t_{k-1}) \tag{29}$$

Measurement update:

$$\mathbf{K}(t_k) = \mathbf{P}^-(t_k)\left[\mathbf{P}^-(t_k) + \mathbf{R}(t_k)\right]^{-1} \tag{30}$$

$$\hat{\mathbf{x}}(t_k) = \hat{\mathbf{x}}^-(t_k) + \mathbf{K}(t_k)\left(\mathbf{z}_2(t_k) - \hat{\mathbf{x}}^-(t_k)\right) \tag{31}$$

$$\begin{aligned}\mathbf{P}(t_k) = &\left(\mathbf{I} - \mathbf{K}(t_k)\right)\mathbf{P}^-(t_k)\left(\mathbf{I} - \mathbf{K}(t_k)\right)^T \\ &+\mathbf{K}(t_k)\mathbf{R}(t_k)\mathbf{K}(t_k)\end{aligned} \tag{32}$$

where $\mathbf{Q}(t_{k-1})$ and $\mathbf{R}(t_k)$ are the estimated variances of RAIM/FDE processed delta position and position measurements, respectively. They are computed using (14), and the resulting covariance matrices are multiplied with their a posteriori covariance factor, computed using (16).

IX. EXPERIMENTAL RESULTS

The performance of the algorithm has been verified with pedestrian navigation tests. Test data was collected from a circular route, in the campus area of the Tampere University of Technology. Two photographs of the environment of the route are shown in Fig. 3. The route is shown on the map in Fig. 4, where the points of the photographs are marked with labels 'a' and 'b'.

The pseudorange and range rate measurements for the testing of the algorithms were obtained using a SiRF Star II GPS receiver. Position estimates were computed from the measurement data using 11 algorithms composed of different combinations of processing alternatives. These combinations are shown in Table 1. The position and velocity estimates were computed using either LS or WLS algorithm. Both the solutions can be processed by RAIM/FDE, independently of each other. If CKF processing was used, velocity solution was required.

The covariance matrices **Q** and **R,** required by the CKF, are computed using (14). In algorithms based on LS solutions, **Q** and **R** are computed using constant values of 0.05^2 and 8^2 in the diagonal elements of **Σ**, respectively**.** In WLS solutions, the diagonal elements of **Σ** are computed using (4) and (1). If the position or velocity is processed by RAIM/FDE, the covariances from (14) are multiplied by the a posteriori covariance factor, as described previously.

The processing steps of the CKF are adjusted according to the final global test result by the RAIM/FDE processing. When the test results do not indicate unreliable solutions, the filtering is carried out as described in (28)-(32). When RAIM/FDE processed velocity is used and the test result indicates unreliable velocity solution, the projection step of the CKF does not change the predicted position estimate, but increases the uncertainty of the estimate by 100^2. Using the large diagonal values of Q in this situation the algorithm reflects the design assumptions; without velocity

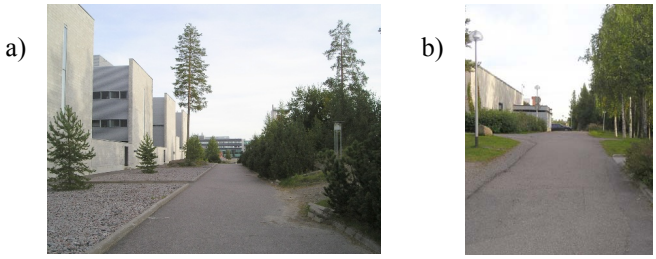

Fig. 3. Environment of the test route

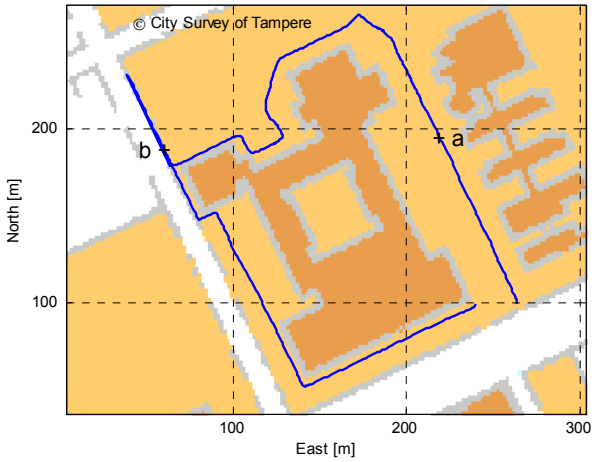

Fig 4. Test route on the map

TABLE I
PERFORMANCE OF THE POSITIONING USING DIFFERENT PROCESSING COMBINATIONS

Algorithm	Processing							Performance		Solutions found inconsistent by RAIM			
	Position			Velocity									
	LS	WLS	RAIM/FDE	LS	WLS	RAIM/FDE	CKF	CTE max [m]	CTE mean [m]	no	pos	vel	pos & vel
LS1	x							51.8	6.3	961			
LS2	x		x					53.3	4.4	945	16		
LS3	x			x			x	54.8	6.8	961			
LS4	x		x	x		x	x	19.6	3.5	858	16	93	6
LS5	x		x	x			x	84.4	5.4	945	16		
WLS1		x						25.2	3.8	961			
WLS2		x	x					25.2	3.5	946	15		
WLS3		x			x		x	9.7	2.9	961			
WLS4		x	x		x	x	x	8.4	3.1	813	15	135	2
WLS5		x	x		x		x	7.7	2.8	946	15		
WLS/LS		x	x	x			x	70.3	3.6	946	15		

measurement, there is very little information about the motion state of the user. In this case, the CKF forgets practically all of its information about the user position and restarts the filtering process from the accuracy of the position measurement. When RAIM/FDE processed position is used and the test result indicates unreliable position solution, the measurement update step of the CKF does not change either position estimate or its uncertainty from the predicted values.

Accuracy of the obtained position solutions was compared with a DGPS position solution, recorded using Thales MobileMappers. As the measure of performance, we used the horizontal distance of the standalone position solution from the DGPS track, i.e. the cross track error (CTE). This performance measure was selected because the reference solution did not contain time tags, thus making the time alignment of the two solutions impossible.

The results of the tests are shown in Table 1. In the performance columns, both the maximum and mean values of the CTE are shown. The last four columns show the number of epochs that yield a specified result in the final global test, i.e. no failures found by RAIM, failures found by position RAIM only, failures found by velocity RAIM only and in the last column, failures found by both position and velocity RAIM. The total number of epochs in the test data was 961. Due to their prediction function, the algorithms with CKF feature provide position estimate every epoch, even if the position or velocity solution or both of them are assessed as unreliable and thus not used by the algorithm, which yields to the increase of the estimation uncertainty.

The CTE results of the algorithms LS1-LS5 show clearly that best results are gained when RAIM/FDE processing is applied on both position and velocity and the results are combined using CKF. The increase of the errors from LS4 to LS5 indicate that some LS velocity solutions rejected by RAIM/FDE in LS4 are indeed erroneous and if accepted for time projection of the position estimate, they cause some large position errors that are not found even in the plain LS solution (LS1). The LS1 and LS4 solutions with the reference solution by DGPS are shown in Fig. 5a.

The effect of the weighting is clear in algorithms WLS1-WLS5: the errors are significantly smaller than with the corresponding LS algorithms. The comparison of the basic LS and WLS solution is shown in Fig. 5b. Applying RAIM/FDE processing to the WLS position gives only a slight improvement to the accuracy, the mean CTE decreases from 3.8 m to 3.5 m (WLS2). Compared to this, the effect of CKF and additional information of the WLS velocity is significant; the maximum CTE drops from 25.2 m to 9.7 m and the mean CTE drops from 3.8 m to 2.9 m (WLS3). Fig. 5c shows that the main improvement by CKF is the decrease of large position errors.

When both the velocity and position are processed by RAIM/FDE before CKF (WLS4), the maximum CTE decreases further to 8.4 m, while the mean CTE is 3.1 m, which is larger than it was without RAIM/FDE processing.

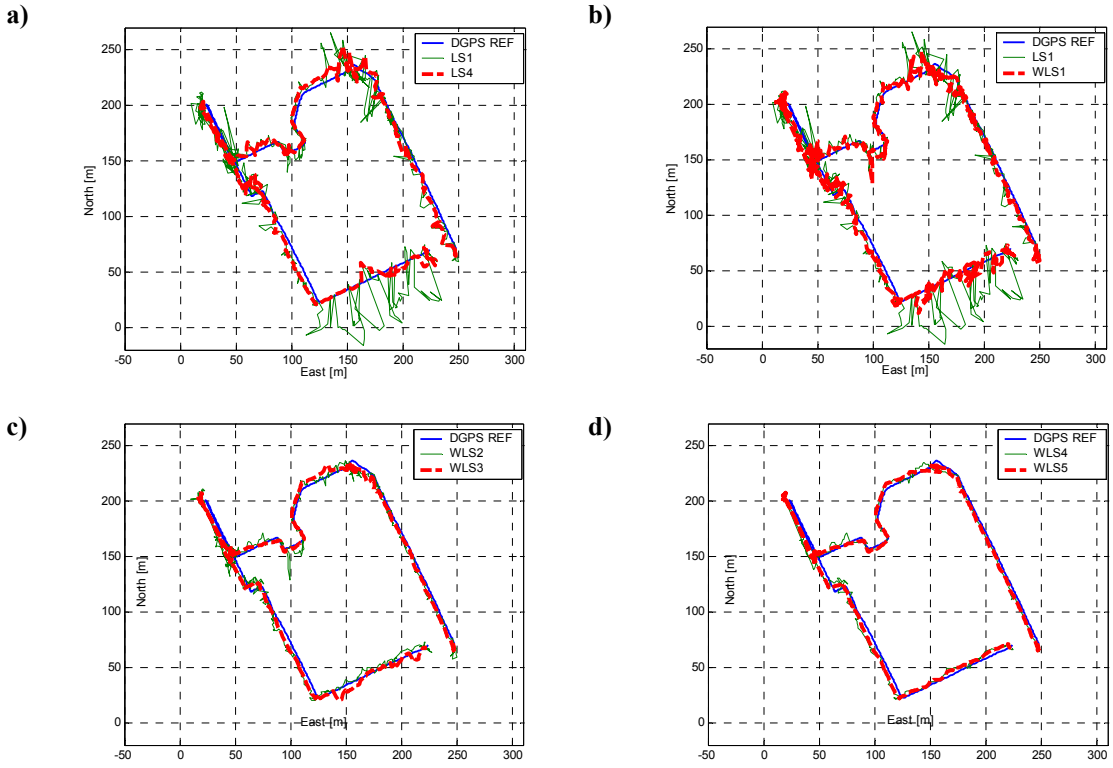

Fig. 5. Position estimates using different algorithms

When CKF is used to combine WLS velocity, without RAIM/FDE processing, and WLS position with RAIM/FDE processing (WLS5), the CTE values decrease further; the maximum CTE to 7.7 m and the mean CTE to 2.8 m (Fig. 5d). Table I shows that in WLS4, velocity estimates of 135 epochs are rejected on the grounds of the RAIM/FDE final global test result. As a consequence of this, the CKF restarts and the previous accuracy achieved by the filtering is lost: 135 epochs out of 961 is quite large amount of missing velocity solutions for the CKF to work properly.

To test the effect of the weighting in velocity solution, we computed CKF estimates using LS velocity and RAIM/FDE processed WLS position (WLS/LS). Using this configuration, the maximum CTE increases to 70.3 m. Comparison of this result with the results of WLS5 verifies the usefulness of the covariance model which is the basis of the weighting.

X. CONCLUSIONS

The pedestrian navigation tests showed that using WLS algorithm instead of LS to solve position and velocity, RAIM/FDE processing of the solutions and fusing them together using CKF improves significantly the accuracy of position estimates. With LS solution of the position, the maximum and mean CTE values were 51.8 m and 6.3 m, respectively. With WLS and RAIM/FDE processed position, the maximum and mean errors were 25.2 m and 3.5 m. Applying CKF on WLS and RAIM/FDE processed position and velocity the values were 8.4 m and 3.1 m. Applying CKF on WLS and RAIM/FDE processed position and WLS velocity the values were 7.7 m and 2.8 m. Thus, adding the CKF to the WLS + RAIM/FDE processing reduces both the maximum and mean errors; the CKF has the largest effect on the maximum errors.

In the test with WLS position and WLS velocity, both RAIM/FDE processed and combined using CKF, 14% of the velocity solutions were rejected by the RAIM final global test. This caused frequent resets of the CKF, resulting in poorer performance than with CKF using RAIM/FDE processed WLS position and WLS velocity without RAIM/FDE processing. This suggests that either the covariance model of delta pseudorange errors or the parameters of RAIM/FDE should be revised. However, the weighting of velocity solution using the same covariance model proved to be beneficial for the CKF.

REFERENCES

[1] Goad, C. G., "Optimal Filtering of Pseudoranges and Phases from Single-Frequency GPS Receivers", NAVIGATION, Journal of The Institute of Navigation, Vol. 39, No. 3, Fall 1990, pp. 249-262.

[2] Hatch, R. R., "The Synergism of GPS Code and Carrier Measurements," Proceedings of the Third International Geodetic Symposium on Satellite Doppler Positioning, Las Cruces, NM, February 1982, pp. 1213-32.

[3] Hwang, P. Y. C., Brown, R. G., "GPS Navigation: Combining Pseudorange with Continuous Carrier Phase Using a Kalman Filter," NAVIGATION, Journal of The Institute of Navigation, Vol. 37, No. 2, Summer 1990, pp. 181-196.

[4] Brown, R. G., Hwang, P. Y. C., Introduction to Random Signals and Applied Kalman Filtering, 3rd ed., John Willey & Sons, Inc., 1997.

[5] Cooper, S., Durrant-Whyte, H., "A Kalman Filter Model for GPS Navigation of Land Vehicles", Proc. of the IEEE/RSJ/GI International Conference on Intelligent Robots and Systems '94. 'Advanced Robotic Systems and the Real World', IROS '94, Munich, Germany, Sept. 12-16, 1994, Vol. 1, pp. 157 – 163.

[6] Syrjärinne, J., Saarinen, J., "An Evaluation of Motion Model Structures within the IMM Frame Using Range only Measurements", Proc. of Int. Conference on Artificial Intelligence, Las Vegas, USA, June 28- July 1, 1999, Vol. I, pp. 254-260.

[7] Leppäkoski , H., Syrjärinne, J., Takala, J., 2003, "Complementary Kalman Filter for Smoothing GPS Position with GPS Velocity," Proc. of ION GPS/GNSS 2003, Portland, Oregon, pp. 1201-1210.

[8] Brown, R. G., "Integrated Navigation Systems and Kalman Filtering: A Perspective," NAVIGATION, Journal of The Institute of Navigation, Vol. 19, No. 4, Winter 1972-73, pp. 355-362.

[9] Kaplan, E. D., (ed.), Understanding GPS: Principles and Applications, Artech House Inc., 1996.

[10] Qi, H., Moore, J. B., 2002, "Direct Kalman Filtering Approach for GPS/INS Integration," IEEE Transactions on Aerospace and Electronic Systems, 38(2), pp. 687 – 693.

[11] Farrell, J., Barth, M., The Global Positioning System and Inertial Navigation, The McGraw-Hill Companies,Inc. 1998.

[12] Brown, R. G., Hagerman, L. L., "An Optimum Inertial/Doppler-Satellite Navigation System," NAVIGATION, Journal of The Institute of Navigation, Vol. 16, No. 3, Fall 1969, pp. 260-270.

[13] Leick A., GPS Satellite Surveying, 3rd Edition, John Wiley and Sons Inc., 2004.

[14] Institute of Navigation, Global Positioning System, Papers Published in NAVIGATION, Vol. V, Special ION Publication on RAIM, 1998.

[15] Teunissen P. J. G., "Quality Control and GPS", in GPS for Geodesy, 2nd Edition, P.J.G. Teunissen and A. Kleusberg, Eds., Springer, New York, NY, 1998, pp. 271-318.

[16] Schaffrin B., "Reliability Measures for Correlated Observations", Journal of Surveying Engineering, Vol. 123, No. 3, Aug. 1997, pp. 126-137.

[17] Kuang S., Geodetic Network Analysis and Optimal Design: Concepts and Applications, Ann Arbor Press Inc., 1996.

[18] Hewitson S., "GNSS Receiver Autonomous Integrity Monitoring: A Separability Analysis", Proc. ION GPS 2003, Portland, OR, USA, Sept. 9-12, 2003, pp. 1502-1509.

[19] Baarda W., A Testing Procedure for Use in Geodetic Networks, Netherlands Geodetic Commission, Publication on Geodesy, New Series 2, No. 5, Delft, Netherlands, 1968.

[20] Lu G., Quality Control for Differential Kinematic GPS Positioning, MSc thesis, Department of Geomatics Engineering, University of Calgary, Calgary, Canada, 1991.

[21] Kuusniemi H., G. Lachapelle, and J. Takala, "Position and Velocity Reliability Testing in Degraded GPS Signal Environments", GPS Solutions, Vol. 8, No. 4, Dec. 2004, pp. 226-237.

[22] Kuusniemi H., G. Lachapelle, and J. Takala, "Reliability in Personal Positioning", Proc. European Navigation Conference 2004, Rotterdam, the Netherlands, May 16-19 2004, 14 pages.

[23] Kuusniemi H. and G. Lachapelle, "GNSS Signal Reliability Testing in Urban and Indoor Environments", Proc. ION NTM 2004, San Diego, CA, USA, Jan. 26-28, 2004, pp. 210-224.

[24] Wieser A., Robust and Fuzzy Techniques for Parameter Estimation and Quality Assessment in GPS, PhD thesis, Graz University of Technology, Graz, Austria, 2001.

[25] Kuusniemi H., User-Level Reliability and Quality Monitoring in Satellite-Based Personal Navigation, PhD thesis, Tampere University of Technology, Tampere, Finland, 2005.